

RESEARCH

Open Access



Natural product myricetin is a pan-KDM4 inhibitor which with poly lactic-co-glycolic acid formulation effectively targets castration-resistant prostate cancer

Jai-Shin Liu^{1,2†}, Wei-Kai Fang^{1,3†}, Shan-Min Yang¹, Meng-Chen Wu¹, Tsan-Jan Chen¹, Chih-Ming Chen^{3,4}, Tung-Yueh Lin¹, Kai-Lun Liu¹, Chien-Ming Wu¹, Yun-Ching Chen⁵, Chih-Pin Chuu⁶, Ling-Yu Wang^{7,8}, Hsing-Pang Hsieh^{3,4,9}, Hsing-Jien Kung^{10,11} and Wen-Ching Wang^{1*} 

Abstract

Background: Castration-resistant prostate cancer (CRPC) with sustained androgen receptor (AR) signaling remains a critical clinical challenge, despite androgen depletion therapy. The Jumonji C-containing histone lysine demethylase family 4 (KDM4) members, KDM4A–KDM4C, serve as critical coactivators of AR to promote tumor growth in prostate cancer and are candidate therapeutic targets to overcome AR mutations/alterations-mediated resistance in CRPC.

Methods: In this study, using a structure-based approach, we identified a natural product, myricetin, able to block the demethylation of histone 3 lysine 9 trimethylation by KDM4 members and evaluated its effects on CRPC. A structure-based screening was employed to search for a natural product that inhibited KDM4B. Inhibition kinetics of myricetin was determined. The cytotoxic effect of myricetin on various prostate cancer cells was evaluated. The combined effect of myricetin with enzalutamide, a second-generation AR inhibitor toward C4-2B, a CRPC cell line, was assessed. To improve bioavailability, myricetin encapsulated by poly lactic-co-glycolic acid (PLGA), the US food and drug administration (FDA)-approved material as drug carriers, was synthesized and its antitumor activity alone or with enzalutamide was evaluated using in vivo C4-2B xenografts.

Results: Myricetin was identified as a potent α -ketoglutarate-type inhibitor that blocks the demethylation activity by KDM4s and significantly reduced the proliferation of both androgen-dependent (LNCaP) and androgen-independent CRPC (CWR22Rv1 and C4-2B). A synergistic cytotoxic effect toward C4-2B was detected for the combination of myricetin and enzalutamide. PLGA-myricetin, enzalutamide, and the combined treatment showed significantly greater antitumor activity than that of the control group in the C4-2B xenograft model. Tumor growth was significantly lower for the combination treatment than for enzalutamide or myricetin treatment alone.

[†]Jai-Shin Liu and Wei-Kai Fang contributed equally to this work

*Correspondence: wawang@gapp.nthu.edu.tw

¹ Institute of Molecular and Cellular Biology and Department of Life Sciences, National Tsing-Hua University, Hsinchu 30013, Taiwan
Full list of author information is available at the end of the article



Conclusions: These results suggest that myricetin is a pan-KDM4 inhibitor and exhibited potent cell cytotoxicity toward CRPC cells. Importantly, the combination of PLGA-encapsulated myricetin with enzalutamide is potentially effective for CRPC.

Keywords: Myricetin, Castration-resistant prostate cancer, Histone lysine demethylase family 4 (KDM4), Poly lactic-co-glycolic acid (PLGA), Enzalutamide

Background

Prostate cancer (PCa) is now the sixth leading cause of cancer-related deaths in men and the first in the UK and second in the United States [1]. Androgen deprivation therapy by surgery or hormonal castration has been the standard treatment for PCa driven by the androgen receptor (AR) pathway since the 1970s [2]. Despite an effective response lasting for a few years, the majority of patients develop a more aggressive form of cancer, referred to as castration-resistant PCa (CRPC). CRPC is primarily stimulated by sustained or even increased AR activity due to AR amplification, AR mutations, and/or the expression of AR splice variants that generate constitutively active forms [3–7] and the upregulation of cytochrome P450 17A1 (CYP17A1), which increases intratumoral androgen synthesis [8]. The second-generation AR antagonist enzalutamide and the inhibitor of CYP17A1, abiraterone, which blocks the synthesis of androgen, have been developed and approved by FDA to improve outcomes for patients with CRPC [8, 9]. While they effectively alleviate symptoms and prolong survival, patients almost always develop resistance, leading to death within a short period. Relapse is common after 1–2 years of treatment and after only 4–6 months in advanced cases (post-chemotherapy) [8, 9]. It is, therefore, necessary to develop a therapeutic modality that can diminish or eliminate aberrantly activated AR activity.

The KDM4 histone lysine demethylase family has recently emerged as a target for tumor therapy [10, 11]. Members of the KDM4/JMJD2 family (KDM4A–KDM4E) catalyze the removal of an *N*_ε-methyl group from *N*_ε-methyl-lysine residues and belong to dioxygenases with α -ketoglutarate (α -KG) and Fe(II) as cofactors [11, 12]. KDM4A, KDM4B, and KDM4C share a similar domain structure (JmjN, JmjC, two plant homeodomains, and two Tudor domains), while KDM4D and KDM4E lack the C-terminal domains (plant homeodomain and Tudor). KDM4A–KDM4C members act on two histone methyl marks, *i.e.*, histone 3 lysine 9 trimethylation/dimethylation (H3K9me3/me2) and histone 3 lysine 36 trimethylation/dimethylation (H3K36me3/me2) [13, 14], whereas KDM4D and KDM4E only demethylate H3K9me3/me2 [14].

KDM4A–KDM4C enzymes are often overexpressed in several types of malignancies, including prostate,

breast, lung, and gastrointestinal tract cancers, lymphoma, and medulloblastoma [10, 15]. Of note, KDM4A and KDM4B interact with AR [16–18]. KDM4A serves as a coactivator of E2F1 [19] and KDM4B regulates AR signaling and turnover to promote tumor progression [17]. KDM4C is upregulated in CRPC [20] and promotes the proliferation of PCa via the activation of c-Myc and AKT [21]. Moreover, KDM4B coactivates c-Jun to regulate the expression of IL-8 [15], enhances autophagy [22], and regulates DNA damage and retrotransposition [23, 24]. By demethylating H3K9me3, a repressive mark enriched in heterochromatin [25, 26], KDM4A–KDM4C function to coactivate AR in the case of PCa, releasing the transcriptional block and promoting tumor progression.

Thus far, two types of KDM4 inhibitors have been reported: α -KG analogues and catalytic-site inhibitors [11]. Of α -KG analogues (*N*-oxalylglycines, hydroxamate analogues, pyridine 2,4-dicarboxylic acids, and 8-hydroxyquinolines), the inhibitor ML324 based on the 8-hydroxyquinoline skeleton shows submicromolar inhibitory activity toward JMJD2E/KDM4E (in vitro), good cell permeability, and in vitro ADME properties [27, 28]. M324 blocks KDM4A-dependent herpes virus-mediated replication in infected cells and displays a promising therapeutic effect by targeting KDM4 [27]. The other 8-hydroxyquinoline -based derivative, B3, blocks the binding of KDM4B to Polo-like kinase 1 to inhibit prostate tumor growth [29]. Recently, potent catalytic-site inhibitors have been developed (Compound 54j and Compound 35) [30, 31]. We have previously identified a catalytic-site inhibitor (NSC636819) that blocks KDM4A/KDM4B-selective inhibition and strongly inhibits LNCaP cell proliferation [18]. However, the in vivo efficacy and other pharmacodynamic features have not been completely characterized.

In this investigation, a natural compound, myricetin, was identified as a pan-KDM4 inhibitor using a structure-guided approach. A poly lactic-co-glycolic acid (PLGA)-encapsulated myricetin was developed to enhance its cytotoxicity and bioavailability. We further compared the effects of PLGA-myricetin, enzalutamide, and their combination of tumor growth in vivo.

Methods

Data mining of KDM4s expression in UCSC Xena and Oncomine

A comparison of the gene expression of normal and tumor in the prostate cohort in TCGA TARGET GTEx was analyzed by using the UCSC Xena browser (<http://xena.ucsc.edu/>). mRNA levels of the primary site and metastatic prostate tumor were compared by using the Grasso prostate dataset in Oncomine analysis tools (<https://www.oncomine.org/resource/login.html>).

Enzyme assay of KDM4

Formaldehyde dehydrogenase (FDH)-coupled demethylase assay was used to determine the demethylase activity as previously described [18]. All tested compounds were dissolved in dimethyl sulfoxide (DMSO; Sigma-Aldrich, St. Louis, MO, USA) at various concentrations and added to the mixture that the final DMSO concentration is 5%. The reagents for demethylase reactions were dissolved in HEPES (Affymetrix Inc., Cleveland, OH, USA) buffer (50 mM, pH 7.5), except Fe(II) solutions, which were made using $(\text{NH}_4)_2\text{Fe}(\text{SO}_4)_2 \cdot 6\text{H}_2\text{O}$ (Sigma-Aldrich) dissolved in 20 mM HCl (Sigma-Aldrich) to make 800 mM stock solution. All the reagents were stored at -30°C . The enzymatic assay was carried out in a final 50 μl reaction mixture containing 50 mM HEPES, pH 7.5, 0.01 U FDH (Sigma-Aldrich), 1 mM NAD^+ (Sigma-Aldrich), 2 μM of demethylase enzyme, 125 μM ascorbate (Sigma-Aldrich), and 10 μM Fe(II), 5% DMSO, and various concentration of H3K9me3 peptide and α -KG. Each reaction was incubated at 25°C for 20 min and the production of NADH was monitored by using the fluorescence spectra (Excitation/Emission: 360/470 nm). All assays were conducted in a 96-well black immune plate (SPL Life Science, Seoul, Korea) and analyzed with a CLARIO star OPTIMA ELISA reader (BMG Labtech., Ortenberg, Germany). The IC_{50} values were obtained by fitting the data to a sigmoid dose–response equation in the GraphPad Prism 7 (GraphPad Software Inc., San Diego, CA, USA).

Virtual screening

All programs were used in BIOVIA Discovery Studio 2018 (BIOVIA, San Diego, CA, USA). The compounds selected from the database were filtered by Lipinski and Veber Rules, and only used Lipinski Rule of Five [32]. Molecular docking analysis was performed with LibDock [33]. Score Ligand Poses module was used to score the compound's poses [34], and the docking analysis of scored compounds was performed using CDocker [35]. KDM4B was used as a protein model (PDB code: 4LXL). The library containing ~60,000 compounds was obtained from the TCM (traditional Chinese medicine) database [36]. Finally, available, virtually optimized

candidates were retrieved for the demethylase enzymatic assay.

Immunoblotting

Total cell lysates were obtained by lysing the cell with buffer [50 mM Tris–HCl pH7.5 (Thermo Fisher Scientific, Waltham, MA, USA), 150 mM NaCl (Honeywell International, Inc., Charlotte, NC, USA), 0.5% Triton X-100 (Sigma-Aldrich), 10% glycerol (Honeywell International, Inc.), 1 mM EDTA (Affymetrix Inc.), and cock-tail protease inhibitors] for 15 min on ice, followed by 10 min of sonication cycle (30 s on, 30 s off) on ice. The level of total histone 3 and trimethylated histone H3K9 was analyzed by western blotting using anti-histone 3 (Cell Signaling, Danvers, MA, USA) and anti-H3K9me3 (Millipore, Burlington, MA, USA).

MTT assay

Cells (3×10^3) were seeded in a 96-well plate 1 day before the treatment. Cell proliferation was measured by MTT colorimetric assay according to the manufacturer's instruction (Roche, Indianapolis, IN, USA).

Drug treatment

Cells were treated with enzalutamide (MDV3100; Active Biochem, Kowloon, Hong Kong, China) and myricetin (Clearsynth, Mumbai, Maharashtra, India), or a combined enzalutamide-myricetin mixture. The IC_{50} value of each drug was determined by treating cells with the drug (0–160 μM) for three days. For combination evaluation, a twofold serial dilution of each drug and its combination points above and below its IC_{50} value was used in an array format. Combination index (CI) values were calculated by CompuSyn software. The values of the combination dose–response curve, which represents drug-effect-shift analysis, were normalized to IC_{50} values of each single molar concentration of drugs (IC_{50} eq), and the plots were generated by Graphpad Prism 7.

Preparation of PLGA-encapsulated myricetin

The single-step precipitation method was employed for the preparation of PLGA formulation containing myricetin. Briefly, myricetin and PLGA were dissolved in an oil solution prepared by 62.1 mg of PLGA (Green Square Materials Inc., Taoyuan, Taiwan), 30 mg of D- α -tocopherol polyethylene glycol 1000 succinate (TPGS; Sigma-Aldrich), 3.1 mg cholesterol (Sigma-Aldrich), 3.1 mg of 1,2-dioleoyl-sn-glycero-3-phosphocholine (DOPC; Avanti Polar Lipids, Alabaster, AL, USA), 6.6 mg 1,2-distearoyl-sn-glycero-3-phosphoethanolamine-N-[methoxy-(polyethyleneglycol)-2000] (ammonium salt) (DSPE-PEG2000; Avanti Polar Lipids), and 0.73 mg of myricetin in 1845 μl of DMSO, and added 308 μl oil into

the 2150 μl of water dropwise under gentle stirring. The mixture was stirred for 30 min at room temperature, followed by centrifugation at 16,220 rpm to collect the PLGA-myricetin formulation. The PLGA particles were re-suspended by adding 150 μl phosphate saline. The myricetin-loaded and empty formulations were centrifuged at 16,220 rpm for 30 min at 25 °C. The pellet was recovered by DMSO and analyzed by Multiskan SkyHigh Microplate Spectrophotometer (Thermo Fisher Scientific) at 380 nm. The absorbance of the myricetin-loaded formation was normalized by subtracting it with the absorbance of empty particles prepared under the same condition.

Xenograft

C4-2B cells (1×10^6 cells) were suspended in a culture medium and mixed with Matrigel Matrix (BD, Franklin Lakes, NJ, USA). The mixtures were implanted subcutaneously into six- to eight-week-old male Balb/c nu/nu mice. When the tumor becomes palpable ($100 \pm 30 \text{ mm}^3$), PLGA-myricetin (intraperitoneal injected, 20 mg/kg, three times a week), enzalutamide (oral gavage feeding, 12.5 mg/kg, five times a week), and the combined treatment were administered respectively. Tumor volumes were measured for up to 3 weeks. The tumor volume was calculated using the formula: length \times width \times height \times 0.52. Statistical analysis was conducted as described below. The animal protocols for mice experiments were approved by National Tsing Hua University Institutional Animal Care and Use Committee (approval number: NTHU-IACUC-10478) and carried out under the institutional guidelines with animal welfare standards.

Statistical analysis

Statistical analyses of cell proliferation, quantitative reverse-transcription PCR (qRT-PCR), and enzymatic experiments were performed by student's *t*-test using the GraphPad Prism 7. The statistical analyses of xenograft analysis were performed by student's *t*-test using the GraphPad Prism 7. A *p*-value < 0.05 was considered statistically significant.

Results

KDM4A, KDM4B, and KDM4C are overexpressed in PCa

We first evaluated the expression of KDM4A, KDM4B, and KDM4C in several prostatic epithelial lines: the immortalized prostatic epithelial line RWPE1, the androgen-dependent PCa line LNCaP, and the AR-positive CRPC lines C4-2, C4-2B, VCaP, and CWR22Rv1. Figure 1A shows that the levels of KDM4A, KDM4B, and KDM4C were much higher in cancer cell lines than in RWPE1. We further evaluated the expression level of

KDM4s in PCa samples (TCGA, $n=495$) and normal samples (GTEx, $n=100$) using the online Xena tool (<https://xenabrowser.net>). As shown in Fig. 1B, levels of KDM4A, KDM4B, and KDM4C were significantly higher in PCa tumors than in normal tissues. Additionally, KDM4A, KDM4B, and KDM4C were significantly higher in the metastatic tumor specimens than in primary tissues based on the Grasso prostate dataset in the OncoPrint database (<https://www.oncoPrint.org/resources/login.html>) (Fig. 1C). These results together suggest that KDM4A/KDM4B/KDM4C are overexpressed in PCa tumors, particularly in metastatic tumors.

Myricetin inhibits KDM4A, KDM4B, and KDM4C, as revealed by a structure-based screening from a natural compound library

Accumulating evidence shows natural products displaying anti-PCa activities [37]. We have thus searched for putative KDM4 inhibitors in the Traditional Chinese Medicine Database@Taiwan [36] guided by a structural-based approach using the KDM4B structure. Compounds ($n=20,781$) were selected from the database ($n=60,563$) based on Lipinski rules of five [32]. LibDock docking program in BIOVIA Discovery Studio [33] was carried out to derive drug-like hits ($n=7565$; LibDock score greater than 120). An additional scoring using the program of Score Ligand Poses [34] obtained 322 hits with LigScore1 and LigScore2 greater than 0. We then carried out docking analysis with CDOCKER [35] to derive the best 23 virtual hits ($-CDOCKER$ Energy greater than 30 kcal/mol and $-CDOCKER$ Interaction Energy greater than 40 kcal/mol) (Additional file 1: Fig. S1). These compounds were subjected to in vitro KDM4B demethylase assay.

Enzymatic analysis of available compounds revealed that three flavonoid compounds (quercetin, kaempferol, and myricetin) exhibited potent inhibitory effects, particularly myricetin and quercetin (relative activity: 5.3% for quercetin, 2.9% for myricetin; IC_{50} : 2.40 μM for quercetin, 1.30 μM for myricetin) (Additional file 1: Table S1). Myricetin, the most potent one, also displayed inhibitory activity toward KDM4A and KDM4C (IC_{50} : 1.13 μM for KDM4A, and 1.12 μM for KDM4C), indicating a pan-KDM4 inhibitor.

We next determined the inhibitory kinetics of myricetin on KDM4A – C. With increasing concentrations of α -KG, myricetin inhibited the demethylation activity of KDM4A, KDM4B, and KDM4C in a competitive manner (Fig. 2A–C). A Lineweaver–Burk plot (Fig. 2A–C) demonstrated myricetin competes with α -KG for binding to the active site ($K_i=0.21 \mu\text{M}$ for KDM4A, 0.53 μM for KDM4B, and 0.15 μM for KDM4C). Kinetic analysis in the presence of increasing concentrations of

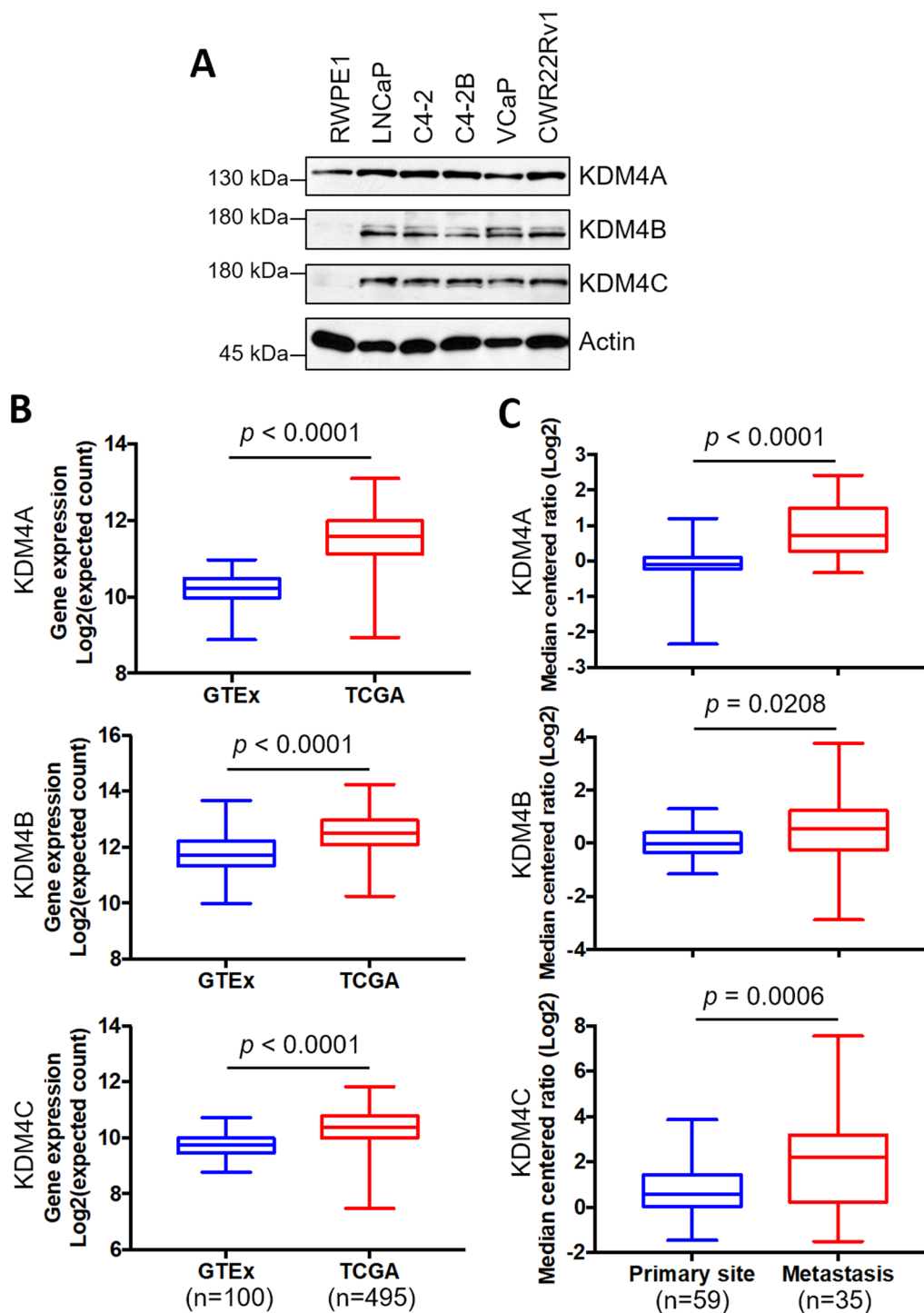
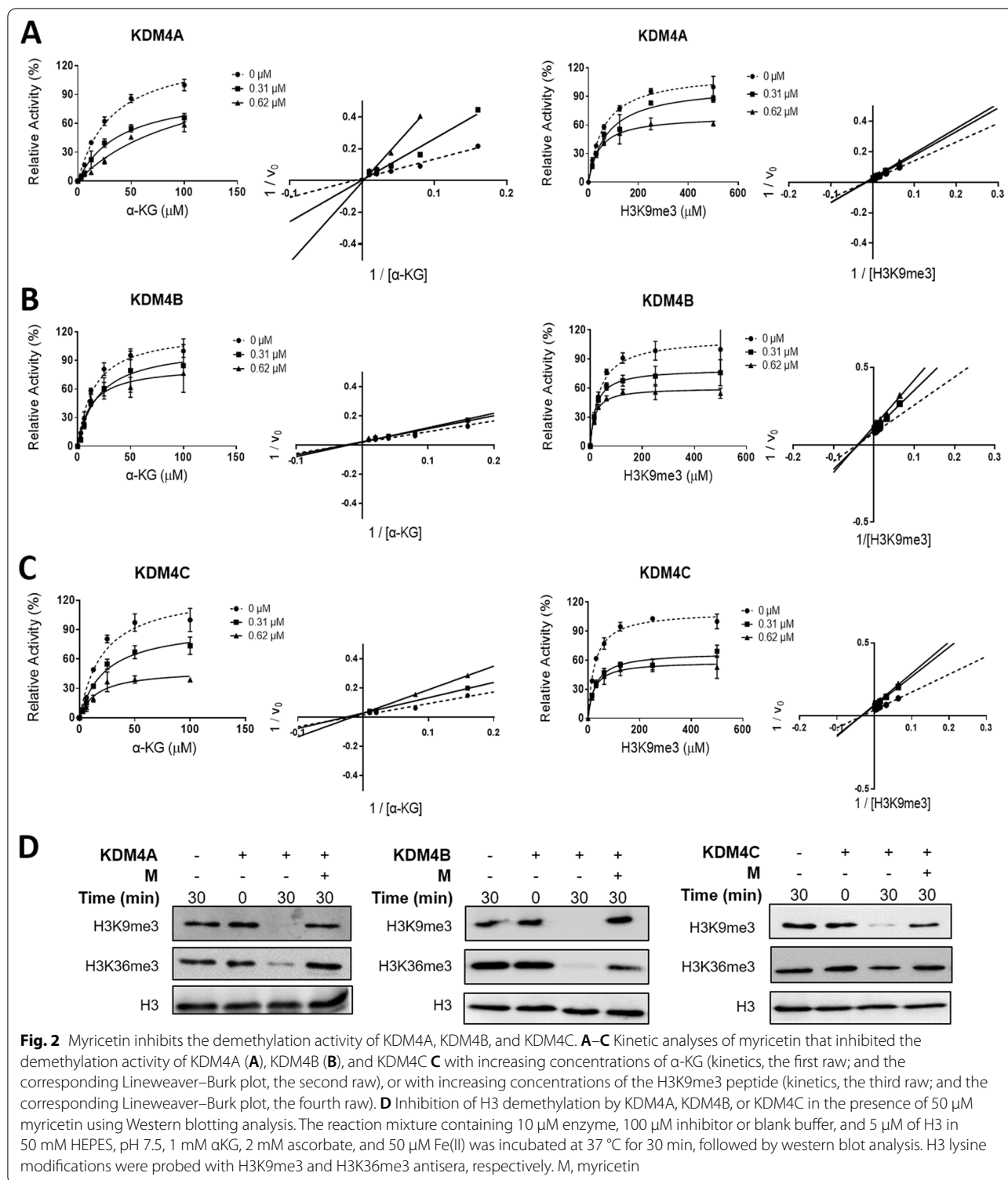


Fig. 1 KDM4A, KDM4B, and KDM4C are overexpressed in PCa. **A** Expression of KDM4A, KDM4B, and KDM4C in an immortalized prostatic epithelial cell line (RWPE1) and PCa cell lines (LNCaP, C4-2, C4-2B, VCaP, and CWR22Rv1) using Western blotting analysis. Actin served as an internal control. **B** Expression of *KDM4A*, *KDM4B*, and *KDM4C* in PCa (TCGA) and normal (GTEx) specimens based on the UCSC Xena tool (<https://xenabrowser.net>). **C** Analysis of expression of *KDM4A*, *KDM4B*, and *KDM4C* in primary and metastatic PCa tissues based on the Grasso prostate dataset in Oncomine database (<https://www.oncomine.org/resource/login.html>). Statistical significance was determined using Student's *t*-test



the H3K9me3 peptide revealed that myricetin blocked the demethylation activity of KDM4A, KDM4B, and KDM4C by a non-competitive mode (Fig. 2A–C; $K_i=1.26 \mu$ M for KDM4A, 1.01 μ M for KDM4B, and

0.62 μ M for KDM4C), indicating that myricetin did not bind to the H3K9me3 peptide-binding region (Fig. 2). Using histones as the substrate, myricetin blocked the

demethylation of H3K9me3 or H3K36me3 by KDM4A, KDM4B, or KDM4C (Fig. 2D).

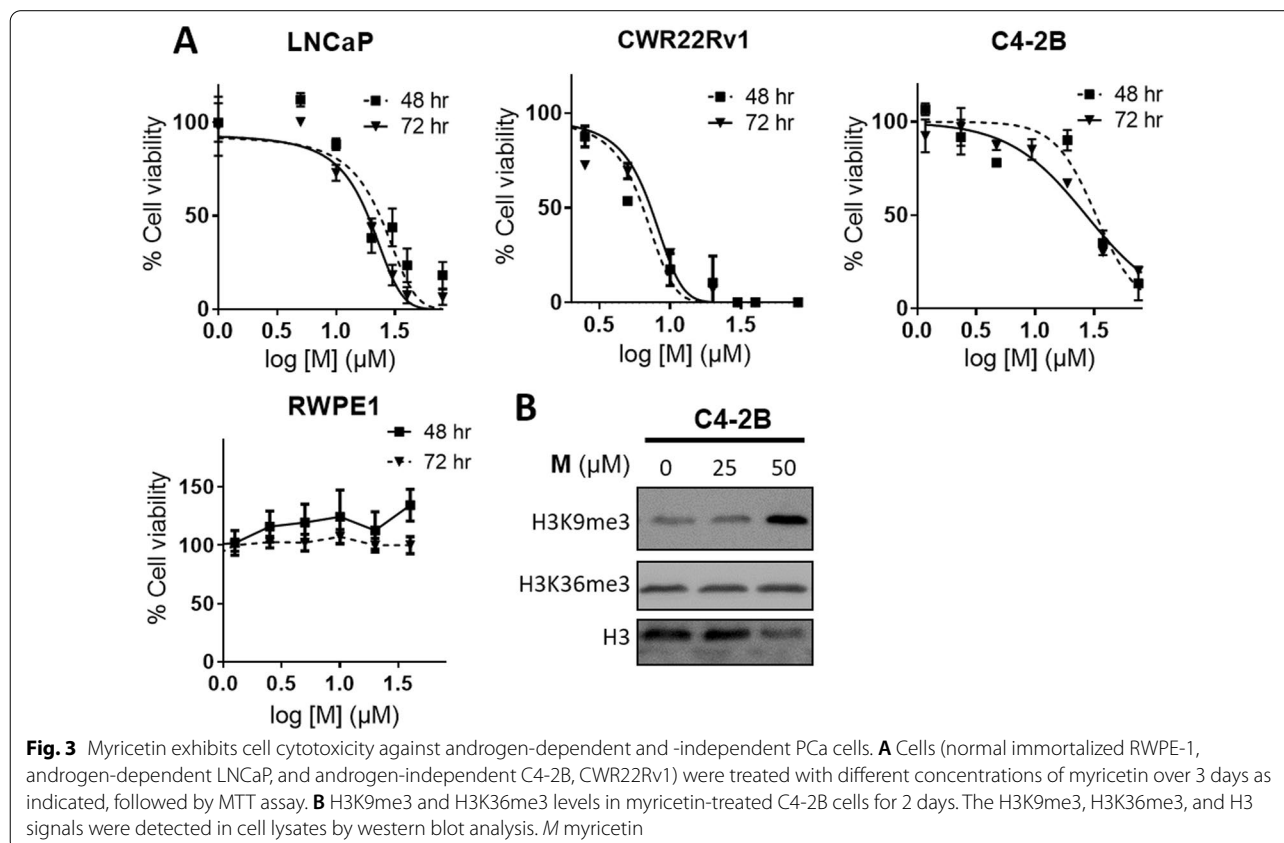
We next performed molecular docking to build a KDM4B·myricetin complex model using BIOVIA, Discovery Studio (CDOCKER) since we were not able to obtain well diffracting myricetin-liganded KDM4 crystals. As shown in Additional file 1: Fig. S2, myricetin occupied the catalytic pocket of KDM4B through extensive H bonds (Asn87, Gly171, Ala187, Asn199, Lys242, Ser289, and Asn291). These seven H bonds form a strong network between myricetin and KDM4B, which makes myricetin a potent inhibitor (Additional file 1: Fig. S2A–B). The 3-hydroxy benzene moiety occupied the α -KG site of KDM4B with four H bonds [18], and the 4H-chromen-4-one moiety of myricetin occupied the other extensive residues in the catalytic pocket of KDM4B with three H bonds and other strong non-bond interactions like Pi-anion (Asp136 and His189) and Pi-Pi stacked interactions (His189) (Additional file 1: Fig. S2A, B).

We further evaluated the inhibitory effects of analogues based on three separate parts of myricetin: (4-phenylpiperazine-1-yl) (phenyl) methanone, (E)-N'-(benzylidene) isonicotinohydrazide, and pyrocatechol (Additional file 1: Tables S2, S3, and S4). Among those,

BPRKD63S0 (3,4-dihydroxybenzoic acid; 63S0) which belongs to an analogue of the pyrocatechol exhibited the highest inhibitory effect (560 nM). In addition, we have determined the crystal structure of the KDM4A·63S0 complex at 2.6 Å (Additional file 1: Table S5; PDB code: 7EQV). The inhibitor 63S0 coordinates the metal ion with two hydroxyl groups and makes two H bonds with Tyr132, Lys206 (Additional file 1: Fig. S3). Superposition of the KDM4A·63S0 crystal structure and the KDM4B·myricetin model revealed the same β -jellyroll structural fold (Additional file 1: Fig. S4A). Additionally, 63S0 and the pyrocatechol moiety of myricetin share overlapped surrounding residues in the α -KG-binding site (Additional file 1: Fig. S4B), consistent with a highly conserved active-site framework seen for the structures of KDM4A–C [18]. These results collectively suggest myricetin interacts with the metal-binding site and serves as a potent α -KG-type inhibitor that blocks KDM4s.

Myricetin effectively inhibits the growth of C4-2B and blocks H3K9me3 demethylation

We evaluated the effect of myricetin on the growth of AR-positive cells. As shown in Fig. 3A, cell viability was significantly reduced in myricetin-treated LNCaP cells after 3 days of culture ($IC_{50} = 18.5 \pm 0.8 \mu\text{M}$). The



proliferation of the CRPC cell line C4-2B was also blocked by myricetin ($IC_{50} = 20.6 \pm 0.9 \mu M$). In contrast, myricetin had essentially no effect on the immortalized normal RWPE-1 line. A higher level of H3K9me3 was observed in C4-2B cells treated with myricetin than in untreated cells, while a comparable H3K36me3 signal was observed, suggesting that myricetin specifically blocked H3K9me3 demethylation in C4-2B cells and reduced cell proliferation (Fig. 3B). These results provide strong evidence that myricetin is a potent natural inhibitor of AR-positive PCa cells (LNCaP and CRPC line C4-2B).

Enzalutamide is a second-generation AR inhibitor for the treatment of metastatic CRPC [38]. Accordingly, we evaluated the effects of combined treatment of enzalutamide with myricetin using the Chou-Talalay method [39]. In particular, we tested the sensitivity of C4-2B using the constant ratio combination design [39]. The combination index (CI) was calculated for the evaluation of synergism (where $CI < 1$ indicated a synergistic effect) [39]. As shown in Fig. 4, the combined drug treatment had a greater inhibitory effect than those of either treatment alone, with low CI values (0.72 ± 0.22), suggesting that the drugs have synergistic effects.

PLGA-encapsulated myricetin formulation plus enzalutamide is more effective than enzalutamide alone

Although myricetin has promising beneficial effects in human cell culture, animal models, and human clinical studies [40], it is poorly absorbed in vivo, possibly owing to its short half-life in plasma [41–43]. To increase its

bioavailability, a polymer-entrapped formulation of myricetin was generated using the FDA-approved drug carrier PLGA which effectively prolongs drug blood circulation, gains enhanced permeability and retention effect for IV injection, and serves as a good platform to conjugate tumor-targeting ligands [44, 45]. The encapsulation efficiency of myricetin in the PLGA formulation was 55%. The PLGA–myricetin displayed greater cytotoxicity than that of free myricetin at $10 - 40 \mu M$ (Fig. 5A).

To assess the efficacy of PLGA–myricetin in vivo, xenografts generated from C4-2B cells were treated with vehicle, PLGA–myricetin, enzalutamide, and the combination of PLGA–myricetin and enzalutamide. As compared with the vehicle, treatment with PLGA–myricetin ($p = 0.0002$), enzalutamide ($p = 0.0002$), or the combination of PLGA–myricetin and enzalutamide ($p = 0.0002$), led to a significant impairment of tumor growth in xenografts at day 13 (Fig. 5B). Significantly, a lower level of tumor volume was detected in the combined treatment than in the PLGA–myricetin treatment ($p = 0.0002$) and in the enzalutamide treatment ($p = 0.0002$) at day 21 (Fig. 5B).

Expression of the proliferation marker Ki-67 was significantly lower in PLGA–myricetin-treated xenografts and enzalutamide-treated xenografts than in the vehicle group (Fig. 5C). The combined treatment, remarkably, exhibited essentially no positive Ki-67 signals (Fig. 5D). We also examined the endothelial cell-specific marker CD31 in xenografts. A significantly higher level of CD31 was detected in the vehicle group than in the PLGA–myricetin-treated and enzalutamide-treated groups (Fig. 5C). Little CD31 was detected in the combined treatment group. These results suggest that PLGA–myricetin effectively blocked the proliferation in C4-2B and xenograft models. Furthermore, the rate of tumor growth was lower for the combined myricetin–enzalutamide treatment than for enzalutamide alone.

Discussion

Accumulating evidence supports the oncogenic potential of KDM4A, KDM4B, and KDM4C, which are over-expressed in several types of cancer, including PCa [10, 11]. Analyses of KDM4B silencing using a lentivirus-based approach or small-drug inhibitors suggest that KDM4B is a potential therapeutic target against androgen-sensitive PCa [18]. Additionally, KDM4B co-activates c-Myc to directly promote c-Myc-mediated tumor metabolism contributing to CRPC progression [46]. Targeting KDM4B thus represents a potential strategy for CRPC driven by c-Myc and AR. In this study, we identified a natural compound, myricetin, capable of blocking KDM4B as well as KDM4A and KDM4C demethylation activity (H3K9me3 and H3K36me3) using a structure-guided approach. We showed that myricetin reduced

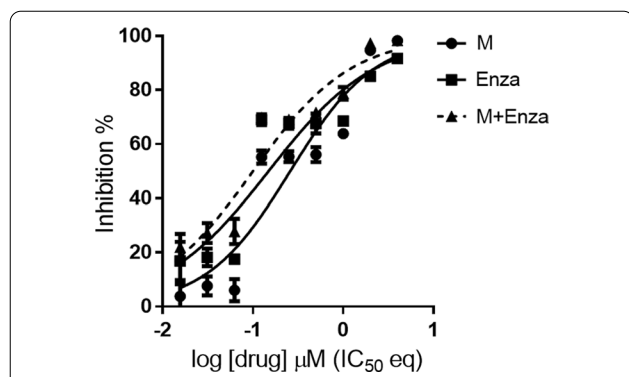


Fig. 4 Effects of myricetin and enzalutamide alone and in combination. C4-2B cells were treated with indicated concentrations of the drugs (M, myricetin; Enza, enzalutamide; M + Enza: the combination of myricetin and enzalutamide). The ratio of Myricetin/enzalutamide is $[IC_{50}]_{Myricetin}/[IC_{50}]_{enzalutamide}$ based on the Chou-Talalay method [39]. Cell viability was measured using the MTT assay, the non-linear regression trendline analysis of IC_{50} values was calculated by Prism7 and the CI values were generated by CompuSyn

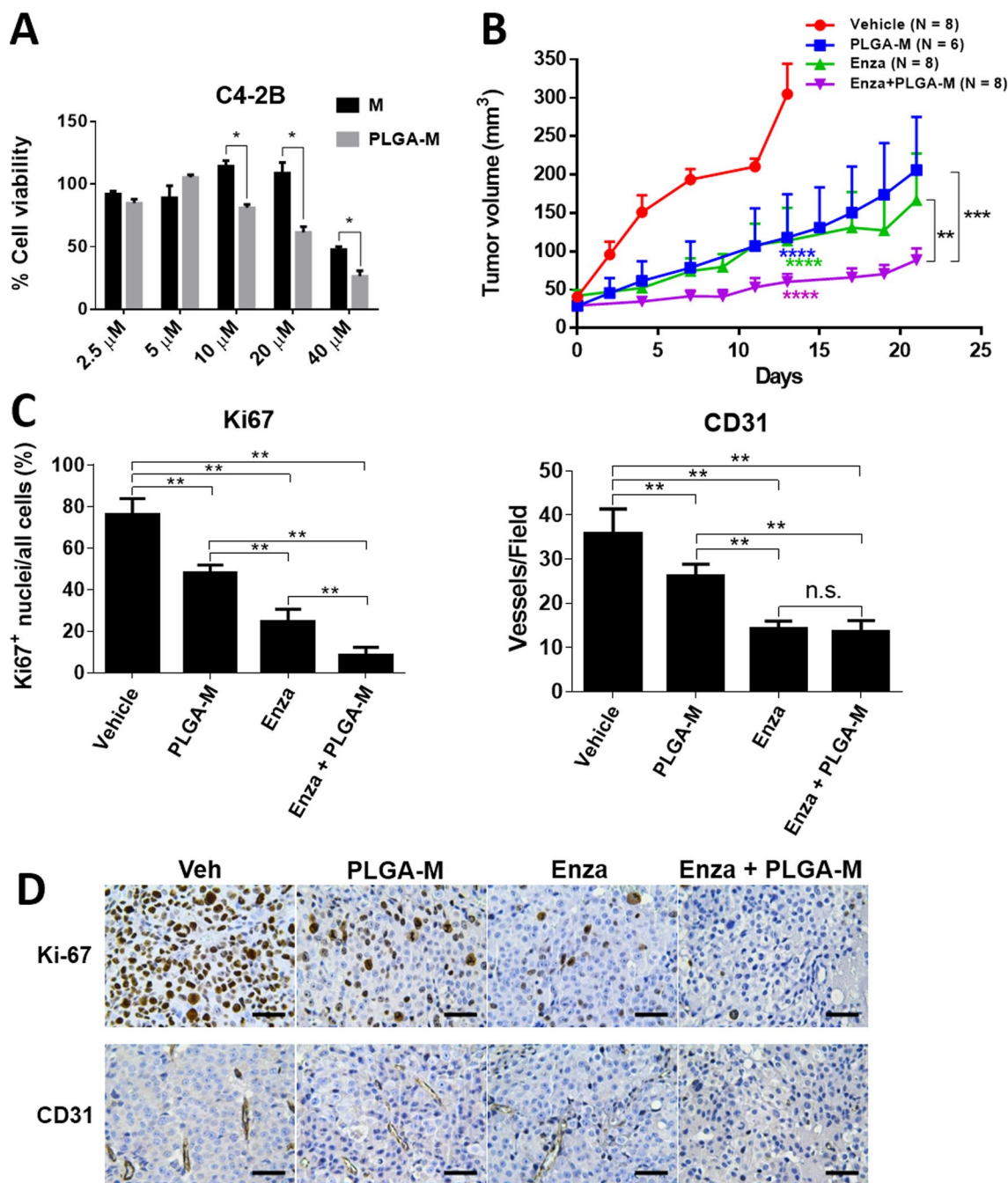


Fig. 5 Myricetin impairs tumor growth in C4-2B xenografts. **A** Comparison of cell viability of C4-2B treated with free-form myricetin (Free M) or PLGA-encapsulated myricetin (PLGA-M). Cells were treated with different concentrations of M or PLGA-M for 24 h, followed by MTT assay. **B** C4-2B cells (1×10^5) were implanted subcutaneously in the hindlimb of nude mice. PLGA-myricetin formulation (PLGA-M) (intraperitoneal injected, 20 mg/Kg, three times a week), enzalutamide (Enza) (oral gavage feeding, 12.5 mg/Kg, five times a week), and the combined treatment (Enza + PLGA-M) were administered respectively after 14 days implantation. Tumor volumes were measured for up to 3 weeks. Tumor volume was calculated using the formula (length \times width \times height \times 0.52). Statistical significance was evaluated using Student's *t*-test. **C** Representative IHC images of Ki67 and CD31 analysis of xenograft tumor sections from mice treated with vehicle, PLGA-M, Enza, or Enza + PLGA-M. **D** The proportion of Ki67 + cell was rescored in each field (400 \times) for six random fields in each group of IHC images. CD31 positive vessels in each field (100 \times) were scored for six random fields in each group. Significance was calculated using Student's *t*-test. **P* < 0.05; ***P* < 0.01; ****P* < 0.001

the growth of androgen-sensitive LNCaP cells as well as androgen-resistant, AR-positive CRPC cell models (CWR22Rv1 and C4-2B), while it did not affect immortalized prostate epithelial cells. Our findings were consistent with the finding that KDM4B downregulation in KDM4B-knockdown C4-2B cells impaired tumor growth in C4-2B xenografts [46]. Of note, KDM4A knockdown or KDM4C knockout in castration-resistant PCa cells also leads to decreased tumor formation [19, 21]. Interestingly, KDM4A, KDM4B, and KDM4C, which share a relatively highly conserved JmjC domain and activity, display overlapping, but distinct spatiotemporal expression profiles. As such, their functions are not completely redundant. They have distinct sets of target genes and work in concert, in a combinatorial and complementary way [47, 48]. Given that both possess oncogenic potential, the development of a pan-KDM4 inhibitor is a promising strategy for advanced PCa.

Three flavonoid compounds (quercetin, kaempferol, and myricetin) displayed the strongest inhibitory effects, particularly myricetin and quercetin (IC_{50} : 1.30 μ M for myricetin and 2.40 μ M for quercetin). A structural difference is noted in the pyrocatechol part of these compounds: myricetin with three -OH groups, quercetin with two, and kaempferol with one. Docking analysis of KDM4B-myricetin reveals higher interaction energy (Additional file 1: Fig. S2). We have thus chosen myricetin for the subsequent analysis. We showed that myricetin exhibits competitive inhibitory activity against α -KG and non-competitive inhibitory activity against the H3K9me3 peptide. A docking simulation revealed that the pyrogallol moiety from myricetin interacts with Ser289 via an H bond and makes Pi-Pi interactions with His189 at the α -KG-binding site, whereas the chromen-4-one moiety makes H bonds with Asn87, Asp136, Gly171, and Lys242 at the peptide-binding region (Additional file 1: Fig. S2) [18, 49]. Additionally, we have determined the KDM4A-63S0 complex structure in which 63S0 is a pyrocatechol analogue. Of note, 63S0 coordinates the metal ion and makes H bonds with Tyr132, Lys206 in the α -KG-binding region of the catalytic pocket. These results collectively suggest myricetin is bound at the center of the active site and functions as a potent α -KG-type inhibitor that blocks the demethylation activity by KDM4s. Importantly, myricetin significantly decreased the viability of AR-positive LNCaP and C4-2B cells. Furthermore, it inhibited histone demethylase activity on H3K9me3 by KDM4A-C in C4-2B cells, suggesting that myricetin is a potent natural compound against demethylation by KDM4A-C in C4-2B cells.

Myricetin, by its nutraceuticals value, has drawn much attention to understanding its molecular mechanisms for medicinal translation. We have shown that myricetin

effectively inhibits the growth of prostate cancer lines LNCaP, C4-2B, and CWR22rv1 but not the immortalized normal RWPE-1. Importantly, we have shown that myricetin which targets KDM4A-C curbs tumor growth in C4-2B xenografts, suggesting an anti-cancer agent in prostate cancer. Chaudhary et al. recently report that flavonoids including myricetin inhibit the enzymatic activity of cytochrome P450 enzymes (CYP1A1 and CYP1B1) [50]. Interestingly, Chaudhary et al. show that myricetin exhibits the highest inhibitory effect using the 2,3,7,8-tetrachlorodibenzo-*p*-dioxin-induced CWR22rv1 cells which constitutively expresses CYP1 enzymes. It is thus possible that myricetin also targets CYP1 enzymes to display an anti-carcinogenic effect, which adds a chemoprotective role of myricetin in prostate cancer prevention. Further investigation is required to clarify the biological targets of myricetin and its underlying mechanisms involved in anti-carcinogenic/anti-proliferative activity in prostate cancer.

Despite the potential health benefits of myricetin including anti-oxidative, anti-inflammatory, anti-cancer, and antidiabetic activities [51], its poor bioavailability through the oral route limits its pharmaceutical application [43]. To overcome this issue, we developed a PLGA-based vehicle for the delivery of myricetin. Notably, PLGA, with its excellent biocompatible and biodegradable features, has been successfully utilized to entrap leuprorelin acetate, an agonist analogue of gonadotropin-releasing hormone, as a lipophilic synthetic polymer microsphere, allowing prolonged release for the treatment of advanced PCa [52–54]. The PLGA-myricetin formulation, interestingly, displayed a lower IC_{50} value toward C4-2B than that of free myricetin, indicating that this form might enhance cellular uptake or penetration [44]. Remarkably, PLGA-myricetin significantly reduced the tumor volume in C4-2B xenografts compared with that in the vehicle group. The combined administration of enzalutamide and myricetin essentially blocked tumor growth in C4-2B xenografts. Furthermore, an *in vitro* efficacy analysis showed that myricetin and enzalutamide have synergistic effects. Thus, targeting the co-activator KDM4 has the potential to control the growth of CRPC driven by the AR pathway. Further investigations are needed to optimize the formulation to increase the synergistic effect *in vivo*.

Conclusions

In summary, a natural compound, myricetin, was identified as a pan-KDM4 inhibitor able to block demethylation activity (H3K9me3 and H3K36me3). Myricetin exhibited potent cell cytotoxicity toward LNCaP as well as CRPC cells (C4-2B and CWR22Rv1) but not toward normal immortalized cells. Importantly, we

provide clear evidence that myricetin encapsulated in PLGA alone or in combination with enzalutamide effectively curbs tumor growth in C4-2B xenografts. Our results highlight a potential intervention strategy for CRPC.

Abbreviations

ADME: Absorption, distribution, metabolism, and excretion; AR: Androgen receptor; CRPC: Castration-resistant prostate cancer; PCa: Prostate cancer; PLGA: Poly lactic-co-glycolic acid; α -KG: α -Ketoglutarate; KDM4: Histone lysine demethylase family 4; CI: Combination index; DMSO: Dimethyl sulfoxide; CYP: Cytochrome P450; H3K9me3/me2: Histone 3 lysine 9 trimethylation/demethylation; H3K36me3/me2: Histone 3 lysine 36 trimethylation/demethylation; qRT-PCR: Quantitative reverse-transcription PCR; TPGS: D- α -tocopherol polyethylene glycol 1000 succinate; DOPC: 1,2-Dioleoyl-sn-glycero-3-phosphocholine; DSPE-PEG2000: 1,2-Distearoyl-sn-glycero-3-phosphoethanolamine-N-[methoxy-(polyethyleneglycol)-2000] (ammonium salt).

Supplementary Information

The online version contains supplementary material available at <https://doi.org/10.1186/s12929-022-00812-3>.

Additional file 1: Fig. S1. Schematic diagram of KDM4B inhibitor discovery from a library of natural products. **Fig. S2.** Analysis of interaction residues in the KDM4B-compound models. (A) The docked KDM4B-myricetin complex. Myricetin, M, occupied the catalytic pocket of KDM4B. (B) 2D diagram of KDM4B-myricetin interaction. Myricetin has seven H bonds, two Pi-anion, one Pi-Pi stacked, one Pi-Pi T-shaped, and one interaction with KDM4B. **Fig. S3.** The $2F_o - F_c$ map of 63S0 in the liganded complex, contoured at 1.5 σ . The bound 63S0 is drawn as heavy blue sticks. The interacting residues are drawn in thin grey sticks. The oxygen and nitrogen atoms are colored in red and blue, respectively. The Nickel ion is drawn in green. **Fig. S4.** Superposition of KDM4A and KDM4B structures. (A) The KDM4A-63S0 crystal structure (orange) and the modeled KDM4B-myricetin structure (slate blue) are superimposed. (B) Superposition of active-site residues based on (A). The bound 63S0 and the nearby residues are shown as thin sticks. Myricetin and the surrounding residues are shown as thick sticks. The oxygen and nitrogen atoms are red and blue, respectively. **Table S1.** Inhibition effect of selected compounds from TCM database on KDM4B. **Table S2.** Inhibition effects of analogues based on a myricetin's fragment, (4-phenylpiperazine-1-yl) (phenyl) methanone, on KDM4A. **Table S3.** Inhibition effects of analogues based on a myricetin's fragment, (E)-N'-(benzylidene) isonicotinohydrazide, on KDM4A. **Table S4.** Inhibition effects of analogues based on a myricetin's fragment, pyrocatechol, on KDM4A. **Table S5.** Crystallographic data and refinement statistics.

Acknowledgements

We thank National Cancer Institute (NCI) for providing the small compounds, Taiwan Bioinformatics Institute Core Facility for assistance in using Oncomine (National Core Facility Program for Biotechnology, MOST 108-2319-B-400-001), and NHRI Laboratory Animal Center and Bi-Juan Wang (NHRI) for the assistance on the animal experiments. We also thank Dr. Ja-An Lin (the University of North Carolina at Chapel Hill) for the support of the statistics of this manuscript.

Author contributions

WCW, HJK, and JSL designed the study. CMC and HPH provided BPRKD compounds. JSL, WKF, TJC, TYL, KLL, and CMW contributed to drug screening and kinetic assay. SMY, MCW, TYL, and LYW carried out cell biology experiments. JSL, MCW, and WKF analyzed the clinical outcome. TYL, KLL, and CPC carried out the xenograft experiments. YCC prepared drug-encapsulated NPs. WCW, HJK, and JSL wrote the manuscript with comments from all authors. All authors read and approved the final manuscript.

Funding

This work was supported by MOST, Taiwan (MOST 105-2314-B-007-001, MOST 106-2314-B-007-001, MOST 107-2314-B-007-001, MOST 108-2320-B-007-001, MOST 108-2311-B-007-006-MY3, MOST 109-2327-B-007-001, and MOST 109-2327-B-007-001, MOST 109-2320-B-007-008, MOST 110-2320-B-007-006 to W.C.W. and MOST 105-2314-B-400-019-MY3, MOST 107-2320-B-038-055-MY3, MOST 105-2320-B-038-071-MY3, MOST 108-2320-B-038-011-MY3 to H.J.K.), as well as TMU Research Center of Cancer Translational Medicine supported by the Featured Areas Research Center Program/Higher Education Sprout Project to H.J.K.

Availability of data and materials

The data presented in the study are included in the article and supplementary information.

Declarations

Ethics approval and consent to participate

All mice were bred and maintained by facility guidelines on animal welfare and with protocols approved by National Tsing Hua University's Institutional Animal Care and Use Committee (Approval Number: NTHU-IACUC-10478).

Consent for publication

Not applicable.

Competing interests

The authors declare no competing interests.

Author details

¹Institute of Molecular and Cellular Biology and Department of Life Sciences, National Tsing-Hua University, Hsinchu 30013, Taiwan. ²Department of Biotechnology and Pharmaceutical Technology, Yuanpei University of Medical Technology, Hsinchu 30015, Taiwan. ³Institute of Biotechnology and Pharmaceutical Research, National Health Research Institutes, Zhunan, Miaoli 35053, Taiwan. ⁴Biomedical Translation Research Center, Academia Sinica, Taipei 11571, Taiwan. ⁵Institute of Biomedical Engineering, National Tsing-Hua University, Hsinchu 30013, Taiwan. ⁶Institute of Cellular and System Medicine, National Health Research Institutes, Zhunan, Miaoli 35053, Taiwan. ⁷Graduate Institute of Biomedical Sciences, Division of Biochemistry, Molecular and Cellular Biology, Chang Gung University, Taoyuan 33302, Taiwan. ⁸Division of Medical Oncology, Chang Gung Memorial Hospital, Linkou, Taoyuan 33305, Taiwan. ⁹Department of Chemistry, National Tsing Hua University, Hsinchu 30013, Taiwan. ¹⁰Department of Biochemistry and Molecular Medicine, University of California Davis School of Medicine, University of California Davis Cancer Centre, Sacramento, CA 95817, USA. ¹¹Graduate Institute of Cancer Biology and Drug Discovery, Taipei Medical University, Taipei 11031, Taiwan.

Received: 20 February 2022 Accepted: 29 April 2022

Published online: 09 May 2022

References

1. Siegel R, Ward E, Brawley O, Jemal A. Cancer statistics, 2011: the impact of eliminating socioeconomic and racial disparities on premature cancer deaths. *CA Cancer J Clin.* 2011;61(4):212–36.
2. Huggins C, Hodges CV. Studies on prostatic cancer. I. The effect of castration, of estrogen and androgen injection on serum phosphatases in metastatic carcinoma of the prostate. *CA Cancer J Clin.* 1972;22(4):232–40.
3. Dehm SM, Schmidt LJ, Heemers HV, Vessella RL, Tindall DJ. Splicing of a novel androgen receptor exon generates a constitutively active androgen receptor that mediates prostate cancer therapy resistance. *Cancer Res.* 2008;68(13):5469–77.
4. Guo Z, Yang X, Sun F, Jiang R, Linn DE, Chen H, Chen H, Kong X, Melamed J, Tepper CG, Kung HJ, Brodie AM, Edwards J, Qiu Y. A novel androgen receptor splice variant is up-regulated during prostate cancer progression and promotes androgen depletion-resistant growth. *Cancer Res.* 2009;69(6):2305–13.
5. Hu R, Dunn TA, Wei S, Isharwal S, Veltri RW, Humphreys E, Han M, Partin AW, Vessella RL, Isaacs WB, Bova GS, Luo J. Ligand-independent androgen

- receptor variants derived from splicing of cryptic exons signify hormone-refractory prostate cancer. *Cancer Res.* 2009;69(1):16–22.
6. Lai CH, Wang HJ, Chang YC, Hsieh WC, Lin HJ, Tang CH, Sheu JJ, Lin CJ, Yang MS, Tseng SF, Wang WC. Helicobacter pylori CagA-mediated IL-8 induction in gastric epithelial cells is cholesterol-dependent and requires the C-terminal tyrosine phosphorylation-containing domain. *FEMS Microbiol Lett.* 2011;323(2):155–63.
 7. Karantanos T, Corn PG, Thompson TC. Prostate cancer progression after androgen deprivation therapy: mechanisms of castrate resistance and novel therapeutic approaches. *Oncogene.* 2013;32(49):5501–11.
 8. Mostaghel EA, Marck BT, Plymate SR, Vessella RL, Balk S, Matsumoto AM, Nelson PS, Montgomery RB. Resistance to CYP17A1 inhibition with abiraterone in castration-resistant prostate cancer: induction of steroidogenesis and androgen receptor splice variants. *Clin Cancer Res.* 2011;17(18):5913–25.
 9. Kim W, Ryan CJ. Androgen receptor directed therapies in castration-resistant metastatic prostate cancer. *Curr Treat Options Oncol.* 2012;13(2):189–200.
 10. Berry WL, Janknecht R. KDM4/JMJD2 histone demethylases: epigenetic regulators in cancer cells. *Cancer Res.* 2013;73(10):2936–42.
 11. Labbé RM, Holowatyj A, Yang ZQ. Histone lysine demethylase (KDM) subfamily 4: structures, functions and therapeutic potential. *Am J Transl Res.* 2014;6(1):1–15.
 12. Klose RJ, Kallin EM, Zhang Y. JmjC-domain-containing proteins and histone demethylation. *Nat Rev Genet.* 2006;7(9):715–27.
 13. Chen Z, Zang J, Whetstone J, Hong X, Davrazou F, Kutateladze TG, Simpson M, Mao Q, Pan CH, Dai S, Hagman J, Hansen K, Shi Y, Zhang G. Structural insights into histone demethylation by JMJD2 family members. *Cell.* 2006;125(4):691–702.
 14. Hillringhaus L, Yue WW, Rose NR, Ng SS, Gileadi C, Loenarz C, Bello SH, Bray JE, Schofield CJ, Oppermann U. Structural and evolutionary basis for the dual substrate selectivity of human KDM4 histone demethylase family. *J Biol Chem.* 2011;286(48):41616–25.
 15. Wu MC, Cheng HH, Yeh TS, Li YC, Chen TJ, Sit WY, Chuu CP, Kung HJ, Chien S, Wang WC. KDM4B is a coactivator of c-Jun and involved in gastric carcinogenesis. *Cell Death Dis.* 2019;10(2):68.
 16. Shin S, Janknecht R. Activation of androgen receptor by histone demethylases JMJD2A and JMJD2D. *Biochem Biophys Res Commun.* 2007;359(3):742–6.
 17. Coffey K, Rogerson L, Ryan-Munden C, Alkharaf D, Stockley J, Heer R, Sahadevan K, O'Neill D, Jones D, Darby S, Staller P, Mantilla A, Gaughan L, Robson CN. The lysine demethylase, KDM4B, is a key molecule in androgen receptor signalling and turnover. *Nucleic Acids Res.* 2013;41(8):4433–46.
 18. Chu CH, Wang LY, Hsu KC, Chen CC, Cheng HH, Wang SM, Wu CM, Chen TJ, Li LT, Liu R, Hung CL, Yang JM, Kung HJ, Wang WC. KDM4B as a target for prostate cancer: structural analysis and selective inhibition by a novel inhibitor. *J Med Chem.* 2014;57(14):5975–85.
 19. Wang LY, Hung CL, Chen YR, Yang JC, Wang J, Campbell M, Izumiya Y, Chen HW, Wang WC, Ann DK, Kung HJ. KDM4A coactivates E2F1 to regulate the PDK-dependent metabolic switch between mitochondrial oxidation and glycolysis. *Cell Rep.* 2016;16(11):3016–27.
 20. Suikki HE, Kujala PM, Tammela TL, van Weerden WM, Vessella RL, Visakorpi T. Genetic alterations and changes in expression of histone demethylases in prostate cancer. *Prostate.* 2010;70(8):889–98.
 21. Lin CY, Wang BJ, Chen BC, Tseng JC, Jiang SS, Tsai KK, Shen YY, Yuh CH, Sie ZL, Wang WC, Kung HJ, Chuu CP. Histone demethylase KDM4C stimulates the proliferation of prostate cancer cells via activation of AKT and c-Myc. *Cancers.* 2019;11(11):1785.
 22. Yang J, Harris AL, Davidoff AM. Hypoxia and hormone-mediated pathways converge at the histone demethylase KDM4B in Cancer. *Int J Mol Sci.* 2018;19(1):240.
 23. Young LC, McDonald DW, Hendzel MJ. Kdm4b histone demethylase is a DNA damage response protein and confers a survival advantage following gamma-irradiation. *J Biol Chem.* 2013;288(29):21376–88.
 24. Xiang Y, Yan K, Zheng Q, Ke H, Cheng J, Xiong W, Shi X, Wei L, Zhao M, Yang F, Wang P, Lu X, Fu L, Lu X, Li F. Histone demethylase KDM4B promotes DNA damage by activating long interspersed nuclear element-1. *Cancer Res.* 2019;79(1):86–98.
 25. Nestorov P, Tardat M, Peters AH. H3K9/HP1 and Polycomb: two key epigenetic silencing pathways for gene regulation and embryo development. *Curr Top Dev Biol.* 2013;104:243–91.
 26. Zhang T, Cooper S, Brockdorff N. The interplay of histone modifications—writers that read. *EMBO Rep.* 2015;16(11):1467–81.
 27. Rai G, Kawamura A, Tumber A, Liang Y, Vogel JL, Ar buckle JH, Rose NR, Dexheimer TS, Foley TL, King ON, Quinn A, Mott BT, Schofield CJ, Oppermann U, Jadhav A, Simeonov A, Kristie TM, Maloney DJ. Discovery of ML324, a JMJD2 demethylase inhibitor with demonstrated antiviral activity in Probe Reports from the NIH Molecular Libraries Program. National Center for Biotechnology Information (US): Bethesda; 2010.
 28. King ON, Li XS, Sakurai M, Kawamura A, Rose NR, Ng SS, Quinn AM, Rai G, Mott BT, Beswick P, Klose RJ, Oppermann U, Jadhav A, Heightman TD, Maloney DJ, Schofield CJ, Simeonov A. Quantitative high-throughput screening identifies 8-hydroxyquinolines as cell-active histone demethylase inhibitors. *PLoS ONE.* 2010;5(11):e15535.
 29. Duan L, Rai G, Roggero C, Zhang QJ, Wei Q, Ma SH, Zhou Y, Santoyo J, Martinez ED, Xiao G, Raj GV, Jadhav A, Simeonov A, Maloney DJ, Rizo J, Hsieh JT, Liu ZP. KDM4/JMJD2 histone demethylase inhibitors block prostate tumor growth by suppressing the expression of AR and BMYB-regulated genes. *Chem Biol.* 2015;22(9):1185–96.
 30. Bavetsias V, Lanigan RM, Ruda GF, Atrash B, McLaughlin MG, Tumber A, Mok NY, Le Bihan YV, Dempster S, Boxall KJ, Jegathanan F, Hatch SB, Savitsky P, Velupillai S, Krojer T, England KS, Seiber J, Thai C, Donovana A, Pal A, Scozzafava G, Bennett JM, Kawamura A, Johansson C, Szykowska A, Gileadi C, Burgess-Brown NA, von Delft F, Oppermann U, Walters Z, Shipley J, Raynaud FI, Westaway SM, Prinjha RK, Fedorov O, Burke R, Schofield CJ, Westwood IM, Bountra C, Muller S, van Montfort RL, Brennan PE, Blagg J. 8-Substituted pyrido[3,4-d]pyrimidin-4(3H)-one derivatives as potent, cell permeable, KDM4 (JMJD2) and KDM5 (JARID1) histone lysine demethylase inhibitors. *J Med Chem.* 2016;59(4):1388–409.
 31. Korczynska M, Le DD, Younger N, Gregori-Puigjane E, Tumber A, Krojer T, Velupillai S, Gileadi C, Nowak RP, Iwasa E, Pollock SB, Ortiz Torres I, Oppermann U, Shoichet BK, Fujimori DG. Docking and linking of fragments to discover jumonji histone demethylase inhibitors. *J Med Chem.* 2016;59(4):1580–98.
 32. Lipinski CA, Lombardo F, Dominy BW, Feeney PJ. Experimental and computational approaches to estimate solubility and permeability in drug discovery and development settings. *Adv Drug Deliv Rev.* 2001;46(1–3):3–26.
 33. Diller DJ, Merz KM Jr. High throughput docking for library design and library prioritization. *Proteins.* 2001;43(2):113–24.
 34. Krammer A, Kirchoff PD, Jiang X, Venkatachalam CM, Waldman M. LigScore: a novel scoring function for predicting binding affinities. *J Mol Graph Model.* 2005;23(5):395–407.
 35. Wu G, Robertson DH, Brooks CL 3rd, Vieth M. Detailed analysis of grid-based molecular docking: a case study of CDOCKER-A CHARMM-based MD docking algorithm. *J Comput Chem.* 2003;24(13):1549–62.
 36. Chen CY. TCM Database@Taiwan: the world's largest traditional Chinese medicine database for drug screening in silico. *PLoS ONE.* 2011;6(1):e15939.
 37. Fontana F, Raimondi M, Marzagalli M, Di Domizio A, Limonta P. Natural compounds in prostate cancer prevention and treatment: mechanisms of action and molecular targets. *Cells.* 2020;9(2):460.
 38. Hoffman-Censits J, Kelly WK. Practical guide to the use of enzalutamide. *Can J Urol.* 2014;21:64–9.
 39. Chou TC. Drug combination studies and their synergy quantification using the Chou-Talalay method. *Cancer Res.* 2010;70(2):440–6.
 40. Thilakarathna SH, Rupasinghe HP. Flavonoid bioavailability and attempts for bioavailability enhancement. *Nutrients.* 2013;5(9):3367–87.
 41. Barve A, Chen C, Hebbar V, Desiderio J, Saw CL, Kong AN. Metabolism, oral bioavailability and pharmacokinetics of chemopreventive kaempferol in rats. *Biopharm Drug Dispos.* 2009;30(7):356–65.
 42. Lin Y, Wu B, Li Z, Hong T, Chen M, Tan Y, Jiang J, Huang C. Metabolite identification of myricetin in rats using HPLC coupled with ESI-MS. *Chromatographia.* 2012;75(11):655–60.
 43. Dang Y, Lin G, Xie Y, Duan J, Ma P, Li G, Ji G. Quantitative determination of myricetin in rat plasma by ultra performance liquid chromatography tandem mass spectrometry and its absolute bioavailability. *Drug Res (Stuttg).* 2014;64(10):516–22.

44. Dinarvand R, Sepehri N, Manoochehri S, Rouhani H, Atyabi F. Polylactide-co-glycolide nanoparticles for controlled delivery of anticancer agents. *Int J Nanomed*. 2011;6:877–95.
45. Allen C, Evans JC. “Hip to be square”: Designing PLGA formulations for the future. *J Control Release*. 2020;319:487–8.
46. Wu MJ, Chen CJ, Lin TY, Liu YY, Tseng LL, Cheng ML, Chuu CP, Tsai HK, Kuo WL, Kung HJ, Wang WC. Targeting KDM4B that coactivates c-Myc-regulated metabolism to suppress tumor growth in castration-resistant prostate cancer. *Theranostics*. 2021;11(16):7779–96.
47. Das PP, Shao Z, Beyaz S, Apostolou E, Pinello L, Angeles AL, O'Brien K, Atsma JM, Fujiwara Y, Nguyen M, Ljuboja D, Guo G, Woo A, Yuan GC, Onder T, Daley G, Hochedlinger K, Kim J, Orkin SH. Distinct and combinatorial functions of Jmjd2b/Kdm4b and Jmjd2c/Kdm4c in mouse embryonic stem cell identity. *Mol Cell*. 2014;53(1):32–48.
48. Pedersen MT, Kooistra SM, Radzishueuskaya A, Laugesen A, Johansen JV, Hayward DG, Nilsson J, Agger K, Helin K. Continual removal of H3K9 promoter methylation by Jmjd2 demethylases is vital for ESC self-renewal and early development. *EMBO J*. 2016;35(14):1550–64.
49. Cascella B, Lee SG, Singh S, Jez JM, Mirica LM. The small molecule JIB-04 disrupts O₂ binding in the Fe-dependent histone demethylase KDM4A/JMJD2A. *Chem Commun (Camb)*. 2017;53(13):2174–7.
50. Chaudhary A, Willett KL. Inhibition of human cytochrome CYP 1 enzymes by flavonoids of St. John's wort. *Toxicology*. 2006;217(2–3):194–205.
51. Semwal DK, Semwal RB, Combrinck S, Viljoen A. Myricetin: A dietary molecule with diverse biological activities. *Nutrients*. 2016;8(2):90.
52. Khan MS, O'Brien A. An evaluation of pharmacokinetics and pharmacodynamics of leuprorelin acetate 3M-depot in patients with advanced and metastatic carcinoma of the prostate. *Urol Int*. 1998;60(1):33–40.
53. Sartor O. Eligard: leuprolide acetate in a novel sustained-release delivery system. *Urology*. 2003;61(2 Suppl 1):25–31.
54. Periti P, Mazzei T, Mini E. Clinical pharmacokinetics of depot leuprorelin. *Clin Pharmacokinet*. 2002;41(7):485–504.

Publisher's Note

Springer Nature remains neutral with regard to jurisdictional claims in published maps and institutional affiliations.

Ready to submit your research? Choose BMC and benefit from:

- fast, convenient online submission
- thorough peer review by experienced researchers in your field
- rapid publication on acceptance
- support for research data, including large and complex data types
- gold Open Access which fosters wider collaboration and increased citations
- maximum visibility for your research: over 100M website views per year

At BMC, research is always in progress.

Learn more biomedcentral.com/submissions

